Numerical Analysis and Validation of the Combined Field Surface Integral Equations for Electromagnetic Scattering by Arbitrary Shaped Two-Dimensional Anisotropic Objects

BENJAMIN BEKER, MEMBER, IEEE, KORADA R. UMASHANKAR, SENIOR MEMBER, IEEE, AND ALLEN TAFLOVE, SENIOR MEMBER, IEEE

Abstract—**The numerical solution of coupled integral equations for arbitrary shaped two-dimensional homogeneous anisotropic scatterers is presented. The theoretical and the numerical approach utilized in the solution of the integral equations is based on the combined field formulation, and is specialized to both transverse electric (TE) and transverse magnetic (TM) polarizations. As opposed to the currently available methods for the anisotropic scatterers, this approach involves integration over the surface of the scatterer in order to determine the unknown surface electric and magnetic current distributions. The solution is facilitated by developing a numerical approach employing the method of moments. The various difficulties involved in the course of the numerical effort are pointed out, and the ways of overcoming them are discussed in detail. The results obtained for two canonical anisotropic structures, namely a circular cylinder and a square cylinder, are given along with validations obtained via alternative methods.**

I. Introduction

In recent years, the solution of physical problems involving anisotropic media has received a great deal of attention. In particular, volumetric approaches such as the finite-difference time-domain (FD-TD) method [1], [2] and the volumetric integral equation method [3]–[5] have already been addressed to solve scattering problems involving anisotropic materials. Also considered was another volumetric method based on the variational principle to solve problems involving anisotropic scatterers [6]. These methods can treat materials characterized by arbitrary permittivity and permeability tensors, thus giving a great deal of freedom in the types of media that can be analyzed by their use. However, the approaches and their numerical schemes [1]–[6] are completely volume dependent, requiring volumetric models even for homogeneous and isotropic cases. Further, their application to electrically large objects has not yet been established. Another approach to the solution of the scattering problem dealing with anisotropic scatterers is based on the plane wave representation of fields in the anisotropic medium [7]. The method discussed in [7] consists of using a superposition type integral to include all possible wave amplitudes and phases, and is applied to the circular cylinder excited at a normal incidence [7], and at an oblique incidence [8]. However, thus far this method has been applied only to the case of a circular cylindrical geometry.

In order to consider arbitrary shapes and computationally manageable sizes of the anisotropic scatterers, an alternative approach to the solution is presented. The method incorporates the surface boundary integrals instead of volume integrals, and is applicable to any arbitrary shaped two-dimensional homogeneous anisotropic scatterers, which can have discontinuities in their surface contour [9]. It involves extension to the formulation of the scattering problem for the isotropic bodies by utilizing the electromagnetic potential theory, and the subsequent derivation of the combined field surface integral equations [10]. However, the derivation of a complete set of consistent potentials for the anisotropic case is much more complicated than the same procedure for the isotropic medium. The detailed derivation of the combined field integral equations is discussed in a separate paper cited earlier [9]. The complete theoretical development is omitted here, and only the most relevant equations are stated to form the starting point for the numerical solution. Due to the complicated nature of these equations, it is practically useful to have a simple numerical scheme for analyzing anisotropic structures, and yet not compromising the accuracy of the numerical results.

The numerical results based on the surface formulation for the transverse magnetic (TM) polarized fields are presented for two canonical anisotropic structures. In general, however, these structures need not be restricted to any particular shape such as a smooth contour. They can include surface discontinuities in the form of sharp corner wedges. Also, in order to

Manuscript received November 19, 1987; revised June 22, 1988; October 26, 1988.

B. Beker and K. R. Umashankar are with the Department of Electrical Engineering and Computer Science, University of Illinois, Chicago, IL 60680.

A. Taflove is with the Department of Electrical Engineering and Computer Science, Technological Institute, Northwestern University, Evanston, IL 60201.

IEEE Log Number 8928391.

0018-926X/89/1200-1573$01.00

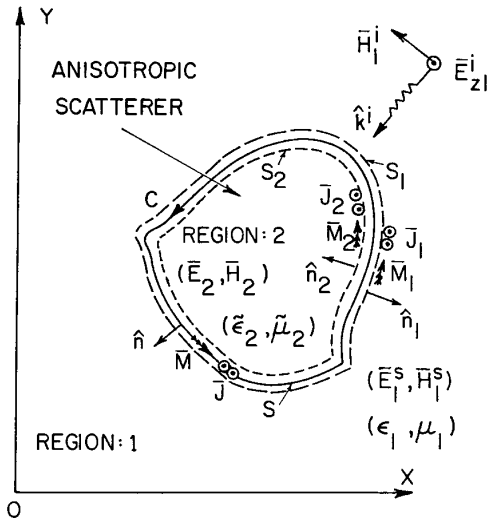

Fig. 1. Geometry of anisotropic scatterer with equivalent current sources.

demonstrate the feasibility of applying the developed method to compute the surface currents and the far fields, a relatively large object with its largest electrical dimension of $k_0 s = 10$ will be considered. In particular, for validating the combined field formulation, the radar cross section (RCS) computed for a circular cylinder is compared to that available in the literature [7]. Also, the near surface current distributions and the RCS of the anisotropic square cylinder are validated against the results obtained based on the FD-TD algorithm [2], [10].

II. Integral Equations for the Surface Fields

Consider a two-dimensional anisotropic object for which there is no variation in its surface contour along the z axis of the coordinate system. It is located in a free-space medium and is excited by an externally incident, TM polarized, field with the time dependence of $e^{-i\omega t}$, where ω is the frequency of the excitation (see Fig. 1). Further, if the excitation is such that the z component of its propagation vector k_z^i is zero, then all scattered field quantities are independent of the z coordinate variation. In order to analyze the complete field distribution due to the presence of the anisotropic object, the equivalence principle [10], [11] can be invoked to obtain a set of coupled (combined field) integral equations for the unknown induced currents on the surface of the object. The full theoretical development leading to those integral equations is presented elsewhere [9], hence, only the key steps are repeated below. Referring to Fig. 1, the equations for the fields internal and external to the anisotropic object can be expressed in terms of the appropriate vector and scalar potentials as is done in [9]–[11]. If the space is separated into two regions, with region 1 occupied by the isotropic (free-space) medium, and the region 2 corresponding to the anisotropic scatterer, respectively, then the total electric E_{z1}^t, and the magnetic $\bar{H}_1^t$ field expressions in the region 1 are given by

$$E_{z1}^t = E_{z1}^i + i\omega A_{z1} - \frac{\hat{z}\cdot(\nabla\times\bar{F}_1)}{\epsilon_1\epsilon_0} \tag{1a}$$

$$\bar{H}_1^t = \bar{H}_1^i + i\omega\bar{F}_1 + \frac{i\omega}{k_1^2}\nabla(\nabla\cdot\bar{F}_1) + \frac{(\nabla\times\bar{A}_1)}{\mu_1\mu_0} \tag{1b}$$

$$k_0^2 = \omega^2\epsilon_0\mu_0 \tag{1c}$$

$$k_1^2 = k_0^2\epsilon_1\mu_1 \tag{1d}$$

where k_1, ϵ_1, μ_1 are the propagation constant, the relative permittivity, and the relative permeability of the isotropic medium. Similarly, the total electric E_{z2}^t and magnetic $\bar{H}_2^t$ fields in the region 2 are given by

$$E_{z2}^t = i\omega A_{z2} - \hat{z}\cdot\frac{\tilde{\epsilon}_2^{-1}}{\epsilon_0}\cdot(\nabla\times\bar{F}_2) \tag{2a}$$

$$\bar{H}_2^t = i\omega\bar{F}_2 + \frac{i\omega}{k_a^2}\nabla(\nabla\cdot(\tilde{\mu}_2\cdot\bar{F}_2)) + \frac{\tilde{\mu}_2^{-1}}{\mu_0}\cdot(\nabla\times\bar{A}_2) \tag{2b}$$

$$k_a^2 = k_0^2\epsilon_{zz}(\mu_{xx}\mu_{yy} + \mu_{xy}^2) \tag{2c}$$

where the relative permittivity and permeability tensors for the anisotropic medium are defined by

$$\tilde{\mu} = \begin{bmatrix} \mu_{xx} & \mu_{xy} & 0 \\ \mu_{yx} & \mu_{yy} & 0 \\ 0 & 0 & \mu_{zz} \end{bmatrix} \tag{3a}$$

$$\tilde{\epsilon} = \begin{bmatrix} \epsilon_{xx} & \epsilon_{xy} & 0 \\ \epsilon_{yx} & \epsilon_{yy} & 0 \\ 0 & 0 & \epsilon_{zz} \end{bmatrix}. \tag{3b}$$

It should be obvious from (1a), (1b) and (2a), (2b) that the appropriate Lorentz-type gauge condition has been utilized to eliminate the magnetic scalar potential, so that the field expressions could be cast in terms of the magnetic and the electric vector potentials only. The derivation leading to the Helmholtz equations and the final integral representation of the required components of the vector potentials $\bar{A}$ and $\bar{F}$ for the anisotropic medium is quite intricate [9]. A detailed account of the procedure taken to obtain them is discussed in [9], [15] and only their final forms are repeated below:

$$A_z(\bar{r}) = -\mu_0\frac{\gamma}{4i\sqrt{\mu_{xx}\mu_{yy}}}\int_C J_z(\bar{r}')H_0^{(1)}(k_a R_m)\,ds' \tag{4a}$$

$$\Xi_x(\bar{r}) = -\epsilon_0\epsilon_{zz}\frac{\gamma}{4i\sqrt{\mu_{xx}\mu_{yy}}}\int_C M_x(\bar{r}')H_0^{(1)}(k_a R_m)\,ds' \tag{4b}$$

$$\Xi_y(\bar{r}) = -\epsilon_0\epsilon_{zz}\frac{\gamma}{4i\sqrt{\mu_{xx}\mu_{yy}}}\int_C M_y(\bar{r}')H_0^{(1)}(k_a R_m)\,ds' \tag{4c}$$

$$\gamma = (\mu_{xx}\mu_{yy} + \mu_{xy}^2) \tag{4d}$$

$$R_m = \sqrt{\frac{(x-x')^2}{\mu_{xx}} + \frac{(y-y')^2}{\mu_{yy}}} \tag{4e}$$

where J_z, M_x, M_y are the unknown electric and magnetic current distributions along the contour C, $H_0^{(1)}$ is the Hankel function of order zero and of first kind, and R_m is the scaled distance parameter [15], [16] between the integration and the observation points with C and ds' representing the contour of the scatterer and its differential element. The quantities Ξ_x

and Ξ_y are the components of the auxiliary vector potential function defined by

$$\bar{\Xi} \equiv \tilde{\mu} \cdot \bar{F} \tag{5}$$

which permits independent differential equations for Ξ_x and Ξ_y, so that eventually solutions for F_x and F_y can be determined [9]. It should be pointed out that in order to obtain the integral solutions for A_z, Ξ_x, Ξ_y it was necessary to demand that the medium tensors possess antisymmetric properties, i.e., $\mu_{xy} = -\mu_{yx}$ for TM polarization, and $\epsilon_{xy} = -\epsilon_{yx}$ for transverse electric (TE) polarization. The corresponding superposition integrals for the external isotropic medium can readily be obtained from (4a)–(4d) and (5) by setting the diagonal elements of the medium tensors (those in (3a) and (3b)) equal and the off-diagonal ones to zero.

Finally, application of the boundary conditions on the tangential components of the total electric and magnetic fields along C, yields the following set of two combined field (coupled) integral equations for the surface currents:

$$-\hat{n} \times \bar{E}_1^i = i\omega(\hat{n} \times \hat{z})(A_{z1} + A_{z2}) - \hat{n} \times \left(\frac{\nabla \times \bar{F}_1}{\epsilon_0 \epsilon_1} + \frac{\tilde{\epsilon}_2^{-1} \cdot (\nabla \times \bar{F}_2)}{\epsilon_0} \right) \tag{6a}$$

$$-\hat{n} \times \bar{H}_1^i = \hat{n} \times \left\{ i\omega(\bar{F}_1 + \bar{F}_2) + i\omega \nabla \left(\nabla \cdot \left(\frac{\bar{F}_1}{k_1^2} + \frac{\tilde{\mu}_2 \cdot \bar{F}_2}{k_a^2} \right) \right) + \left(\frac{(\nabla \times \bar{A}_1)}{\mu_1 \mu_0} + \frac{\tilde{\mu}_2^{-1} \cdot (\nabla \times \bar{A}_2)}{\mu_0} \right) \right\} \tag{6b}$$

which are valid for the TM polarized incident field $(\bar{E}_1^i, \bar{H}_1^i)$. The same equations also apply to the TE polarization following appropriate substitutions of symbols as is dictated by the duality principle [11]. In particular, allowing $\bar{E} \rightarrow \bar{H}$, $\bar{H} \rightarrow -\bar{E}$, and interchanging the roles of the permittivity and permeability tensors results in the desired combined field integral equations set for the TE polarization.

III. Numerical Solution of the Integral Equations

The first step in the numerical solution of (6a) and (6b) based on the method of moments is the proper choice of the testing and the expansion functions. This choice is usually dictated by the complexity of the integrals and the scatterer contour. For example, if the integrands contain derivatives with respect to the observation coordinates along the tangential direction of the scatterer, then it is customary to use higher order testing functions, such as the triangles, to replace those derivatives by differences [12]. The use of the simpler testing functions, such as pulses, simplifies the testing scheme. On the other hand, it complicates the integrands, because the derivative operations due to the gradient, divergence, and the curl will now be taken inside the integrals. However, this approach has been found to speed up the convergence rate of the

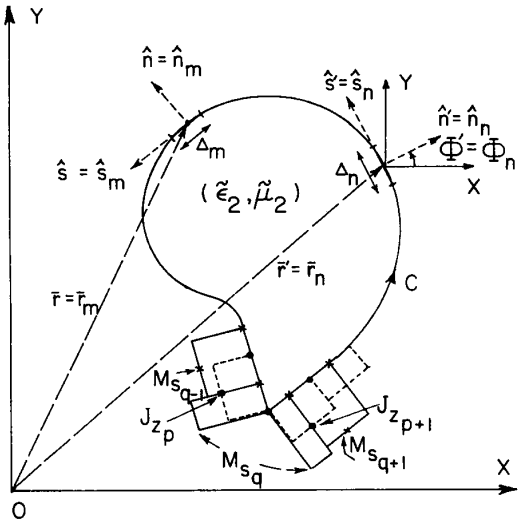

Fig. 2. Segmented boundary contour.

The expansion scheme for the unknown surface electric and magnetic currents is chosen to consist of the simplest possible functions, such as pulses. The only remaining task is to decide whether the pulses for each current expansion ought to be staggered or not. This, in fact, depends on the contour of the scatterer, i.e., if the contour is smooth (continuous), then there is no need to use the staggered distribution. However, if the contour includes surface discontinuities, such as the corners and arbitrary bends, then it is appropriate to stagger the pulses so as to enforce the continuity of the circumferential current, and to avoid expanding the axial current at the bend where it is singular [10]. For the problem at hand, i.e., for TM polarization, the axial electric current J_z, and the circumferential magnetic current M_s, are expanded in a staggered manner as shown in Fig. 2, because objects having both smooth and discontinuous contours can be considered for the solution using the same computer algorithm. These same expansion pulses are also employed as the testing functions for the two coupled integral equations. Thus, the unknown surface currents are expanded as

$$J_z(\bar{r}') = \sum_{n=1}^{n=N} p_n^J(\bar{r}') J_{zn} \tag{7a}$$

$$M_s(\bar{r}') = \sum_{n=N+1}^{n=2N} p_n^M(\bar{r}') M_{sn} \tag{7b}$$

where $p_n^J(\bar{r}')$ and $p_n^M(\bar{r}')$ are the unit pulse functions which can also serve as the testing functions $t^E(\bar{r})$ and $t^H(\bar{r})$ in the reduction procedure of the integral operators in (6a) and (6b) to a matrix form, i.e.,

$$t^E(\bar{r}) = \sum_{m=1}^{m=M} p_m^J(\bar{r}) \tag{8a}$$

$$t^H(\bar{r}) = \sum^{m=2M} p_m^M(\bar{r}) \tag{8b}$$

where (8a) and (8b) are used in taking the inner products with (6a) and (6b), respectively. The resulting system of the matrix equations, following testing and expansion, turns out to be

$$\begin{bmatrix} [Z^E_{mn}] & [Y^E_{mn}] \\ [Z^H_{mn}] & [Y^H_{mn}] \end{bmatrix} \begin{bmatrix} [J_{zn}] \\ [M_{sn}] \end{bmatrix} = \begin{bmatrix} [E^i_{zm}] \\ [H^i_{sm}] \end{bmatrix} \tag{9}$$

where the various elements of the system submatrices are defined below.

1) The elements of the impedance matrix of the $\bar{E}$ field equation:

$$[Z^E_{mn}] = \frac{k_0\eta_0}{4}\int_{\Delta_n}\left[\mu_1 H_0^{(1)}(k_1 R) + \frac{\gamma}{\sqrt{\mu_{xx}\mu_{yy}}} H_0^{(1)}(k_a R_m)\right] ds'. \tag{10a}$$

2) The elements of the admittance matrix of the $\bar{E}$ field equation:

$$[Y^E_{mn}] = \frac{1}{4i}\int_{\Delta_n} k_1(\hat{n}'\cdot\hat{R})H_1^{(1)}(k_1 R)\,ds' + \frac{1}{4i}\int_{\Delta_n}\frac{k_a}{\sqrt{\mu_{xx}\mu_{yy}}}[(\hat{n}'\cdot\bar{R}) + \mu_{xy}(\hat{s}'\cdot\bar{R}_{m'})] \cdot \frac{H_1^{(1)}(k_a R_m)}{R_m}\,ds'. \tag{10b}$$

3) The elements of the impedance matrix of the $\bar{H}$ field equation:

$$[Z^H_{mn}] = \frac{\eta_0}{k_0 i}\int_{\Delta_n}(\hat{n}\cdot\hat{R})k_1 H_1^{(1)}(k_1 R) + \frac{\eta_0}{k_0 i}\int_{\Delta_n}\frac{k_a}{\sqrt{\mu_{xx}\mu_{yy}}}[(\hat{n}\cdot\bar{R}) - \mu_{xy}(\hat{s}\cdot\bar{R}_{m'})] \cdot \frac{H_1^{(1)}(k_a R_m)}{R_m}\,ds'. \tag{10c}$$

4) The elements of the admittance matrix of the $\bar{H}$ field equation:

$$\begin{aligned}[Y^H_{mn}] = \frac{\epsilon_1}{2}\int_{\Delta_n}\Bigg[&\cos(\Phi_m - \Phi')H_0^{(1)}(k_1 R) \\ &- \left(\sin\Phi_m \sin\Phi'\left(1 - \frac{2(x_m - x')^2}{R^2}\right)\right. \\ &+ \cos\Phi_m\cos\Phi'\left(1 - \frac{2(y_m - y')^2}{R^2}\right) \\ &\left. + \frac{2\sin(\Phi_m + \Phi')(x_m - x')(y_m - y')}{R^2}\right) \\ &\cdot H_2^{(1)}(k_1 R)\Bigg]\,ds' \\ &+ \frac{\epsilon_{zz}}{\sqrt{\mu_{xx}\mu_{yy}}}\int_{\Delta_n}(\mu_{yy}\sin\Phi_m\sin\Phi' + \mu_{xx}\cos\Phi_m\cos\Phi' \\ &+ \mu_{xy}\sin(\Phi_m - \Phi'))H_0^{(1)}(k_a R_m)\,ds' \\ &- \frac{\epsilon_{zz}\gamma}{2(\mu_{xx}\mu_{yy})^{3/2}}\int_{\Delta_n}\Bigg[(\mu_{yy}\sin\Phi_m\sin\Phi' \\ &+ \mu_{xx}\cos\Phi_m\cos\Phi')H_0^{(1)}(k_a R_m) \\ &+ \left(\mu_{yy}\sin\Phi_m\sin\Phi'\left(1 - \frac{2(x_m - x')^2}{\mu_{xx}R_m^2}\right)\right. \\ &+ \mu_{xx}\cos\Phi_m\cos\Phi'\left(1 - \frac{2(y_m - y')^2}{\mu_{yy}R_m^2}\right) \\ &\left. + \frac{2\sin(\Phi_m + \Phi')(x_m - x')(y_m - y')}{R_m^2}\right) \\ &\cdot H_2^{(1)}(k_a R_m)\Bigg]\,ds'. \end{aligned} \tag{10d}$$

5) The column excitation matrix of the $\bar{E}$ field equation:

$$[E^i_{zm}] = \hat{z}\cdot\bar{E}^i(\bar{r}_m). \tag{10e}$$

6) The column excitation matrix of the $\bar{H}$ field equation:

$$[H^i_{sm}] = \frac{4\eta_0}{k_0}\hat{s}(\bar{r}_m)\cdot\bar{H}^i(\bar{r}_m) \tag{10f}$$

and where $[J_{zn}]$ and $[M_{sn}]$ are the unknown surface electric and magnetic current column matrices along the tangential directions $\hat{z}$ and $\hat{s}$ of the contour C. In (10a)–(10d), the subscripts m and n refer to the observation and the integration points on the scatterer contour C, and in the above matrix elements,

$$\bar{R}_m = \frac{(x_m - x')}{\sqrt{\mu_{xx}}}\hat{x} + \frac{(y_m - y')}{\sqrt{\mu_{yy}}}\hat{y} \tag{11a}$$

$$\bar{R}_{m'} = \frac{(x_m - x')}{\mu_{xx}}\hat{x} + \frac{(y_m - y')}{\mu_{yy}}\hat{y} \tag{11b}$$

$$\bar{R} = (x_m - x')\hat{x} + (y_m - y')\hat{y} \tag{11c}$$

with R_m, $R_{m'}$, R being their respective magnitudes, and with $\hat{n}$, $\hat{n}'$, $\hat{s}$, $\hat{s}'$ being the normal and the tangential unit vectors on the contour at either the observation or the integration points (see Fig. 1). These unit vectors are defined in the following manner:

$$(\hat{n};\,\hat{n}') = \cos(\Phi;\,\Phi')\hat{x} + \sin(\Phi;\,\Phi')\hat{y} \tag{11d}$$

$$(\hat{s};\,\hat{s}') = -\sin(\Phi;\,\Phi')\hat{x} + \cos(\Phi;\,\Phi')\hat{y} \tag{11e}$$

where Φ and Φ' are the angles between the normals $\hat{n}$ and $\hat{n}'$ and the x axis of the coordinate system.

It is evident from (10a)–(10d), that as a consequence of letting the various differential operations to be performed on the Green's function inside the integrals, results in the appearance of higher order Hankel functions, in particular $H_2^{(1)}$. Nevertheless, the complications arising in the evaluation of the system submatrices due to such an approach, are outweighted by the gain in the quicker convergence rate of the solution [13]. Otherwise, the evaluation of those submatrices is straightforward apart from the calculation of their singular values, which should be obtained asymptotically. A detailed mathematical analysis leading to the determination of the singular parts of the various integrals is presented in [15], and

only the final results are summarized in the following. First, for the anisotropic medium they are given by

$$I_1 = \int_{\Delta_m} H_0^{(1)}(k_a R_m)\, ds' = \Delta_m \int_0^1 H_0^{(1)}\left(\frac{(\beta\bar{\Delta}_m)s}{2}\right) ds \tag{12a}$$

which is a well-known integral and can be evaluated in numerous ways [14]. The singular values of integrals involving the first derivative of $H_0^{(1)}$ are given by

$$I_2 = \frac{k_a \mu_{xy}}{4i\sqrt{\mu_{xx}\mu_{yy}}} \int_{\Delta_m} (\hat{s}' \cdot \bar{R}_{m'}) \frac{H_1^{(1)}(k_a R_m)}{R_m}\, ds' \to 0 \tag{12b}$$

$$I_3 = \frac{k_a}{4i\sqrt{\mu_{xx}\mu_{yy}}} \int_{\Delta_m} (\hat{n}' \cdot \bar{R}) \frac{H_1^{(1)}(k_a R_m)}{R_m}\, ds' \to \frac{1}{2} \tag{12c}$$

where all of the vectors have been defined previously in (11a)–(11e), and it should also be noted that the values of these integrals are same irrespective of whether the medium is anisotropic or isotropic. The most complicated integrals contain the second derivatives of $H_0^{(1)}$, nevertheless they can be evaluated asymptotically to yield the following results:

$$I_4 = \int_{\Delta_m} \left(1 - \frac{2(x_m - x')^2}{\mu_{xx} R_m^2}\right) H_2^{(1)}(k_a R_m)\, ds'$$
$$= \frac{\bar{\Delta}_m(\cos^2 \bar{\Phi}_m - \sin^2 \bar{\Phi}_m)}{\sqrt{\mu_{yy} \sin^2 \Phi_m + \mu_{xx} \cos^2 \Phi_m}} \left[\frac{(\beta\bar{\Delta}_m)^2}{96} + i\frac{16}{\pi(\beta\bar{\Delta}_m)^2}\right] \tag{12d}$$

$$I_5 = \int_{\Delta_m} \left(1 - \frac{2(y_m - y')^2}{\mu_{yy} R_m^2}\right) H_2^{(1)}(k_a R_m)\, ds' = -I_4 \tag{12e}$$

$$I_6 = \int_{\Delta_m} \left[\frac{2\sin(\Phi_m + \Phi')(x_m - x')^2 (y_m - y')^2}{R_m^2}\right] \cdot H_2^{(1)}(k_a R_m)\, ds'$$
$$= -\frac{\sqrt{\mu_{xx}\mu_{yy}}(\bar{\Delta}_m \sin \bar{\Phi}_m \cos \bar{\Phi}_m)}{\sqrt{\mu_{yy} \sin^2 \Phi_m + \mu_{xx} \cos^2 \Phi_m}} \left[\frac{(\beta\bar{\Delta}_m)^2}{96} + i\frac{16}{\pi(\beta\bar{\Delta}_m)^2}\right] \tag{12f}$$

where the the angle $\bar{\Phi}_m$ is defined in [15] and related to the real angle Φ_m by

$$\tan \bar{\Phi}_m = \sqrt{\frac{\mu_{yy}}{\mu_{xx}}} \tan \Phi_m. \tag{12g}$$

The remaining terms β and $\bar{\Delta}_m$ are given by

$$\beta = \frac{k_a}{\sqrt{\mu_{xx}\mu_{yy}}} \tag{12h}$$

$$\bar{\Delta}_m = \Delta_m \sqrt{\mu_{yy} \sin^2 \Phi_m + \mu_{xx} \cos^2 \Phi_m}. \tag{12i}$$

Secondly, the same equations (12a)–(12f) can be specialized for the isotropic medium by simply making appropriate substitution of variables, i.e.,

$$\epsilon_{zz} \to \epsilon_1; \mu_{xx} = \mu_{yy} \to \mu_1; \mu_{xy} \to 0; \bar{\Phi} \to \Phi. \tag{12j}$$

Also, it should be pointed out that the value of $I_3 \to -I_3$ when the external isotropic medium is considered. This is a direct consequence of the observation point approaching the contour in the limit from the opposite direction for the external medium, as opposed to the internal medium, considered above. The remaining integrals are independent of this fact, thus requiring no additional sign changes.

The matrix equations derived above ((9) and (10)) have been programmed on the IBM 370 computer using Fortran 77, and the various quantities of interest, such as the near surface current distributions and the far scattered fields, are calculated in order to analyze the electromagnetic behavior of two-dimensional anisotropic material objects.

IV. Numerical Results

In this section selected numerical results are presented regarding the computed near and far fields, as well as the CPU time required to obtain them based on the solution of the matrix equations (9). Two canonical cylindrical anisotropic geometries are considered, namely the circular and square cylinders excited by an external TM polarized plane wave. Both the near and the far fields are computed, and validated for each of the two geometries. The radar cross section of a circular anisotropic cylinder with $k_0 a = \pi/2$, where a is the radius of the cylinder, characterized by $\epsilon_{zz} = 2$, $\mu_{xx} = 1$, and $\mu_{yy} = 4$ is computed based on the surface integral equation formulation and is compared to the one obtained based on the plane wave superposition integral representation of the fields inside the anisotropic medium [7]. The two results are displayed in Fig. 3 and appear to be in an excellent agreement. Similarly, Fig. 4 illustrates the RCS computed for a circular cylinder of the same size, but with the following anisotropic medium parameters: $\epsilon_{zz} = 2$, $\mu_{xx} = 1$, $\mu_{yy} = 4$, and $\mu_{xy} = -\mu_{yx} = 2$. For both cases, the surface electric and magnetic currents were calculated as well, but are reported elsewhere [15]. The number of unknowns for each of the surface currents was 60, such that the total system matrix size is 120×120 for the level of agreement shown in Fig. 3.

The next case analyzed numerically is a square anisotropic cylinder characterized by $\epsilon_{zz} = 1.5$, $\mu_{xx} = 1.5$, $\mu_{yy} = 2$ whose electrical size is $k_0 s = 10$, where s is the side length of the square. Once again the RCS is computed based on the solution of the combined field equations and is shown in Fig. 5(a). These results are compared with those computed via the FD-TD [10]. The agreement between the RCS patterns calculated by the two methods is quite good except for a small angular range in the shadow region in the interval of 200°–220°. The magnitudes of the surface electric and magnetic currents for this square cylinder are displayed in Figs. 5(b) and 5(c). The level of agreement for the currents is also seen to be good except in the vicinity of the corners of the scatterer where the results of the two methods differ. This discrepancy deserves additional comments. Since the exact nature of the field behavior at the corners of the anisotropic

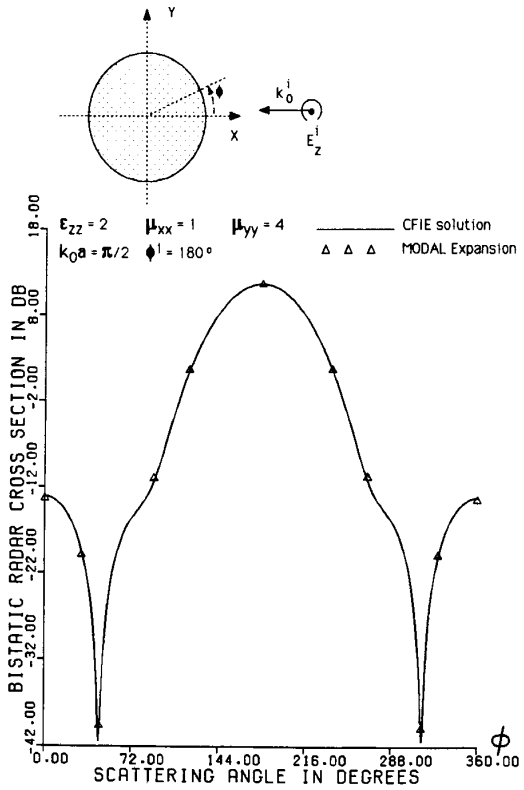

Fig. 3. Bistatic RCS of the circular anisotropic cylinder with only diagonal terms.

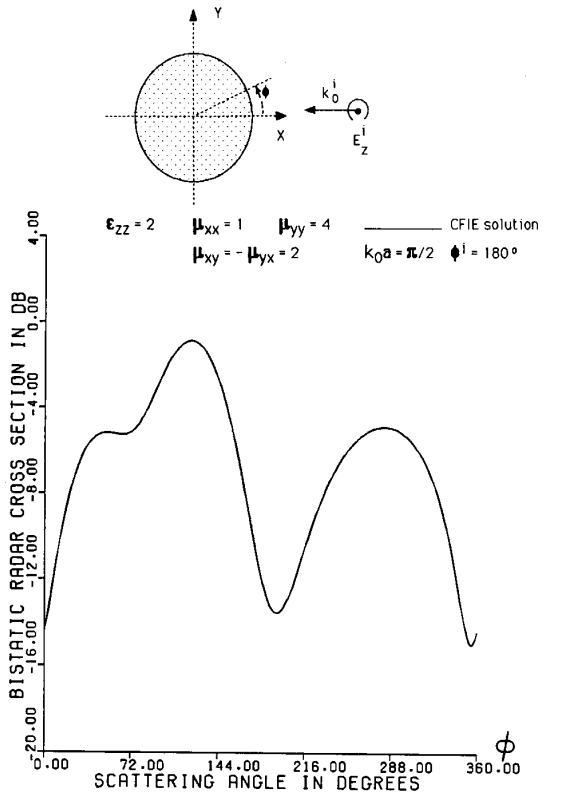

Fig. 4. Bistatic RCS of the circular anisotropic cylinder with mutual permeability terms.

object is not yet known, it is difficult to say with absolute certainty which of the two methods gives the correct result. However, these corner regions are very small compared to the wavelength and since the far scattered fields are not expected to be greatly influenced by the currents over these localized corner regions, the RCS patterns may be more appropriate indicators of the agreement between the two methods. Also to be noted is the fact that in the FD-TD algorithm the fields are computed half a cell away from the actual physical boundary of the object, which may also be responsible for the discrepancies between the results. Since the fields do not vary greatly half a cell away from the object in regions far from surface discontinuities from their values computed directly on the object's surface, the agreement in the results calculated via both methods is expected to be good. However, in regions close to the bends the fields are expected to vary quite a bit between their values half a cell away from the contour and directly on it. This could possibly explain the differences in the results obtained via the two techniques in the vicinity of the corners of the square. The next example considered is a square cylinder having higher permeability values of the medium given by: $\epsilon_{zz} = 2$, $\mu_{xx} = 2$, $\mu_{xx} = 4$, and $k_0 s = 5$. The RCS is computed and compared with that determined by FD-TD (see Fig. 6(a)). The corresponding magnitudes of the surface electric and magnetic currents for this scatterer are shown in Figs. 6(b) and 6(c), respectively. It is worth noting that in this case the results of both methods appear to predict similar behavior of M_s close to the bends in the contour, particularly, both indicate the dip in the magnitude of M_s, but not to the same extent. However, the discrepancy for the axial electric current is still present in those regions. This behavior may be attributed to the sparse sampling of the FD-TD algorithm, which in this case consisted in fifty cells per side of the square. It is believed that even further agreement in the results of the two methods could be achieved by increasing the sampling rate of the FD-TD. It is also worth mentioning that since both FD-TD and surface integral equation approach are based on methods of numerical analysis, it is not realistic to expect both of them to yield identical results. Additional examples for which both the surface currents and the RCS have been computed are available in [15]. The two square cylinders considered here are electrically large structures, especially the first one ($k_0 s = 10$) for which the number of current samples is such that the system matrix is 592×592. Nevertheless, the numerical solution is feasible, because most of the time is consumed by the system matrix inversion (which can be reduced for symmetric objects) and not for matrix filling. It should be pointed out that the symmetry of the structure has not been incorporated in the present algorithm. If the symmetry is incorporated into the algorithm, then substantial reduction in the CPU time for the matrix inversion can be achieved. Further savings in the CPU time can also be obtained if the inversion subroutine, based on the Gaussian elimination, is to perform partial pivoting instead of full pivoting.

In order to provide some idea of the time involved for the computations to obtain the results for the square cylinder dis-

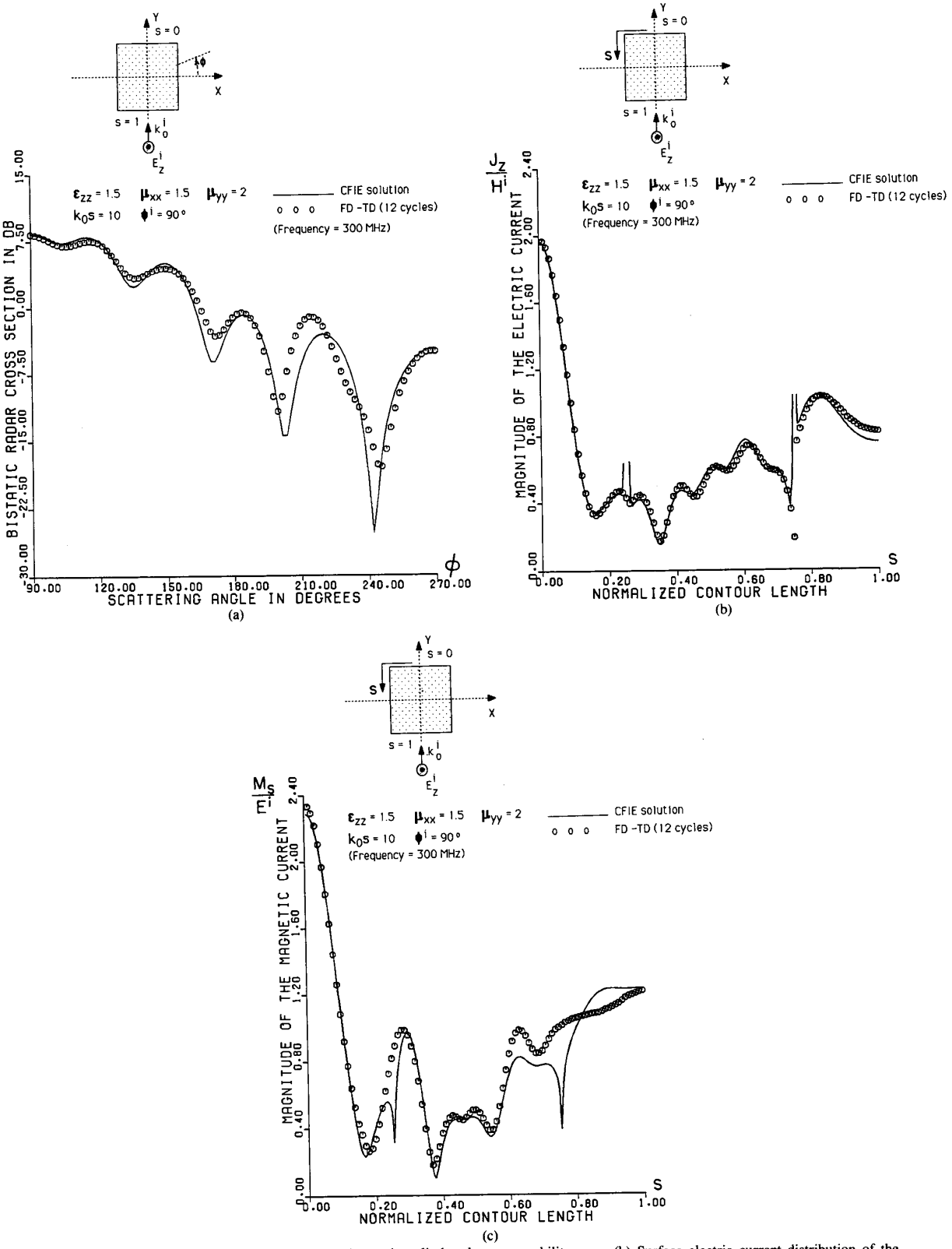

Fig. 5. (a) Bistatic RCS of the square anisotropic cylinder, low permeability case. (b) Surface electric current distribution of the square anisotropic cylinder, low permeability case. (c) Surface magnetic current distribution of the square anisotropic cylinder, low permeability case.

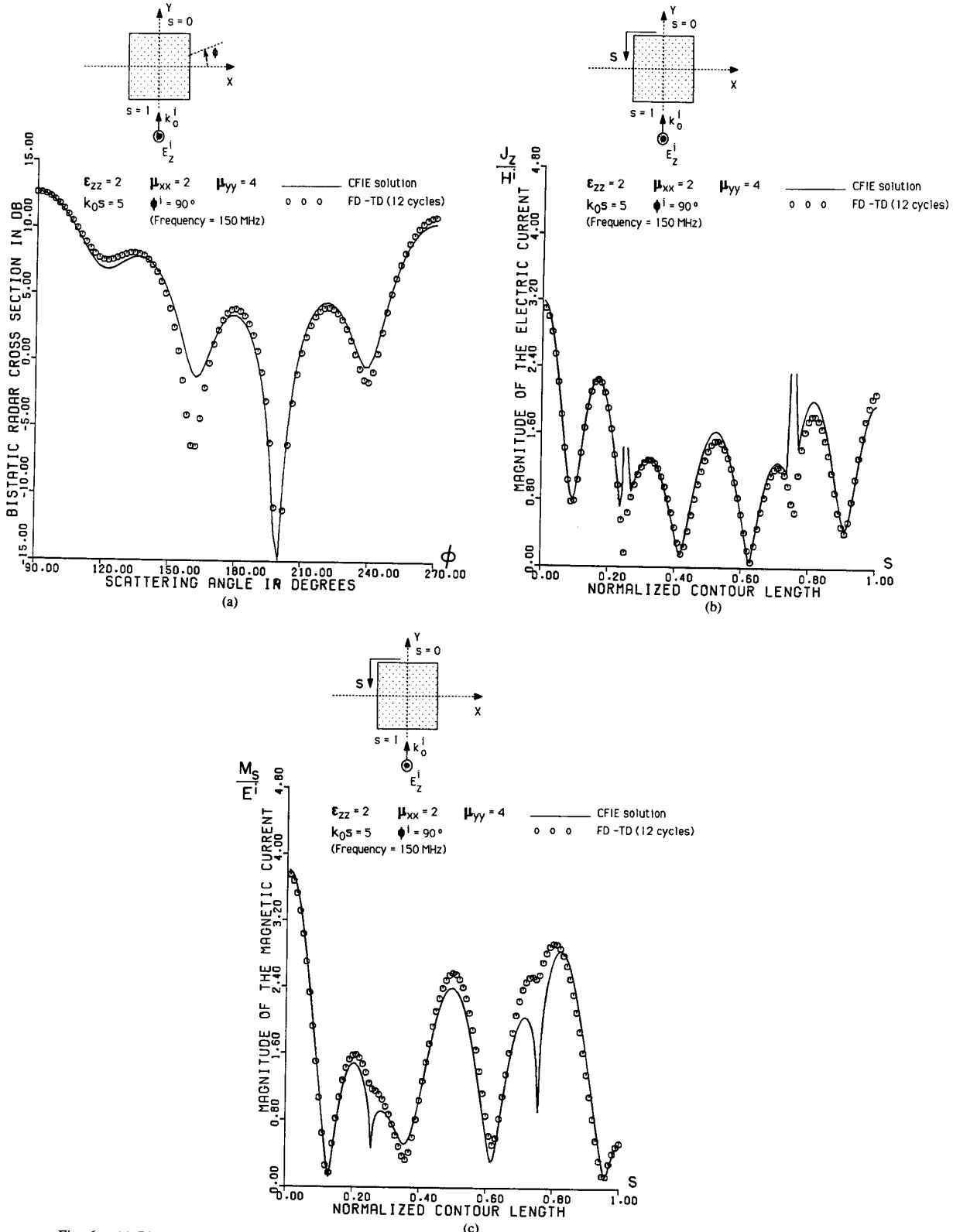

Fig. 6. (a) Bistatic RCS of the square anisotropic cylinder, high permeability case. (b) Surface electric current distribution of the square anisotropic cylinder, high permeability case. (c) Surface magnetic current distribution of the square anisotropic cylinder, high permeability case.

played in Fig. 5, the CPU time consumed by the algorithm was recorded. The actual time for all of the results to be calculated was found to be 1770.10 s on the IBM-370 mainframe. This indicates that consideration of electrically large anisotropic scatterers is quite feasible for the numerical solution.

V. Summary

In this paper, a numerical solution of the combined field surface integral equations for the case of arbitrary shaped two-dimensional anisotropic scatterers has been presented. The computed results for the surface fields and the far scattered fields are validated by the currently available alternative methods, such as the FD-TD [2] and that of plane wave representation of fields in the anisotropic medium [7]. The discussion included a detailed account of the various aspects involved in the numerical solution, including the results of the singularity analysis for the integrals containing different orders of the Hankel functions for both anisotropic and isotropic media. The computer algorithm developed is applicable both for smooth contours and those with sharp edges.

References

[1] A. Taflove and M. E. Brodwin, "Numerical solution of steady-state electromagnetic scattering problems using the time dependent Maxwell's equations," *IEEE Trans. Microwave Theory Tech.*, vol. MTT-23, no. 8, pp. 623–630, Aug. 1975.

[2] A. Taflove and K. R. Umashankar, "Radar cross section of general three-dimensional scatterers," *IEEE Trans. Electromagn. Compat.*, vol. EMC-25, no. 4, pp. 433–440, Nov. 1983.

[3] R. D. Graglia, "Integral equations for anisotropic scatterers," Ph.D. dissertation, Univ. Illinois, Chicago, 1983.

[4] R. D. Graglia and P. L. E. Uslenghi, "Electromagnetic scattering from anisotropic materials, Part I: General theory," *IEEE Trans. Antennas Propagat.*, vol. AP-32, no. 4, pp. 867–869, Aug. 1984.

[5] ——, "Electromagnetic scattering from anisotropic materials, Part II: Computer code and numerical results in two-dimensions," *IEEE Trans. Antennas Propagat.*, vol. AP-35, no. 2, pp. 225–232, Feb. 1987.

[6] R. B. Wu and C. H. Chen, "Variational reaction formulation of scattering for anisotropic dielectric cylinders," *IEEE Trans. Antennas Propagat.*, vol. AP-34, no. 5, pp. 640–646, May 1986.

[7] J. C. Monzon and N. J. Damaskos, "Two-dimensional scattering by a homogeneous anisotropic rod," *IEEE Trans. Antennas Propagat.*, vol. AP-34, no. 10, pp. 1243–1249, Oct. 1986.

[8] J. C. Monzon, "Three-dimensional scattering by an infinite homogeneous circular cylinder: A spectral approach," *IEEE Trans. Antennas Propagat.*, vol. AP-35, no. 6, pp. 670–682, June 1987.

[9] B. Beker and K. R. Umashankar, "Analysis of electromagnetic scattering by arbitrary shaped two-dimensional anisotropic objects: Combined field surface integral equation formulation," *Electromagn.*, vol. 9, pp. 215–229, Jan. 1989.

[10] K. R. Umashankar and A. Taflove, "Analytical models for electromagnetic scattering," Electromagn. Sci. Div., RADC, Hanscom AFB, MA, Final Tech. Rep. June 1984.

[11] R. F. Harrington, *Time-Harmonic Electromagnetic Fields*. New York: McGraw-Hill, 1961, ch. 3.

[12] D. R. Wilton and C. M. Butler, "Effective methods for solving integral and integro-differential equations," *Electromagn.*, vol. 1, no. 3, pp. 289–308, July-Sept. 1981.

[13] B. Beker and K. R. Umashankar, "Numerical solution of the combined field surface integral equations for the analysis of electromagnetic scattering by arbitrary shaped two-dimensional structures," in *Proc. IEEE-AP/URSI Int. Symp.*, Blacksburgh, VA, June 1987, p. 253.

[14] M. Abramowitz and A. I. Stegun, *Handbook of Mathematical Functions*. New York: Dover, 1970, p. 480.

[15] B. Beker, "Analysis of electromagnetic scattering by arbitrary shaped anisotropic objects using combined field surface integral equation formulation," Ph.D. dissertation, Univ. Illinois, Chicago, 1988.

[16] M. Kobayashi and R. Terakado, "New view on an anisotropic medium and its application to transformation from anisotropic to isotropic problems," *IEEE Trans. Microwave Theory Tech.*, vol. MTT-27, no. 9, pp. 769–775, Sept. 1979.

Benjamin Beker (S'83–M'83–M'88), for a photograph and biography please see page 1257 of the November 1987 issue of this Transactions.

Korada R. Umashankar (S'69–M'75–SM'81), for a photograph and biography please see page 765 of the June 1986 issue of this Transactions.

Allen Taflove (M'75–SM'84), for a photograph and biography please see page 766 of the June 1986 issue of this Transactions.